Author(s): Nikitin, Dmitri; Kaur, Balpreet; Preis, Sergei; Dulova, Niina

Title: Degradation of Antibiotic Vancomycin by UV Photolysis and Pulsed Corona Discharge Combined with Extrinsic Oxidants

Year: 2023

Version: Published version

Please cite the original version:

Nikitin, D., Kaur, B., Preis, S., & Dulova, N. (2023). Degradation of Antibiotic Vancomycin by UV Photolysis and Pulsed Corona Discharge Combined with Extrinsic Oxidants. Catalysts, 13(3), Article 466. https://doi.org/10.3390/catal13030466

Degradation of Antibiotic Vancomycin by UV Photolysis and Pulsed Corona Discharge Combined with Extrinsic Oxidants

Dmitri Nikitin [1], Balpreet Kaur [2], Sergei Preis [1] and Niina Dulova [1,*]

[1] Department of Materials and Environmental Technology, Tallinn University of Technology, Ehitajate tee 5, 19086 Tallinn, Estonia
[2] Department of Chemistry, University of Jyväskylä, Survontie 9 B, P.O. Box 35, FI-40014 Jyväskylä, Finland
* Correspondence: niina.dulova@taltech.ee

Abstract: Antibiotics are the most frequently detected pharmaceuticals in the environment creating conditions for the development of resistant genes in bacteria. Degradation and mineralization of glycopeptide antibiotic vancomycin (VMN) were examined by UV photolysis, pulsed corona discharge (PCD), and their combinations with extrinsic oxidants, hydrogen peroxide (HP), peroxydisulfate (PDS), and peroxymonosulfate (PMS). Both combinations were effective in VMN degradation and faster at pH 11 than in acidic or neutral media. Combined with the UV photolysis, HP showed a higher oxidation rate than other oxidants, whereas PMS and PDS proved to be more efficient in combinations with PCD. In contrast to low-to-moderate mineralization of VMN in the UV/oxidant combinations, PCD and PCD/oxidant combinations appeared to be more effective, reaching up to 90% of TOC removal in acidic/neutral solutions. Application of extrinsic oxidants resulted in an energy efficiency of VMN 90% oxidation improved from 36 to 61 g kW^{-1} h^{-1} in HP-assisted photolysis, and from 195 to 250 g kW^{-1} h^{-1} in PCD with additions of HP and PDS, thus showing the promising character of the combined treatment.

Keywords: advanced oxidation; energy efficiency; non-thermal plasma; persulfate

1. Introduction

In recent years, antibiotics, becoming the most frequently detected pharmaceutical compounds in the environment [1], have created conditions for the development of resistant genes in bacteria [2,3]. The resistant bacteria are of increasing concern due to their ecotoxicological effects [4,5]. Vancomycin (VMN) is an amphoteric glycopeptide antibiotic used to treat infections caused by Gram-positive organisms [6]. This antibiotic and its modifications are considered as drugs of last resort, i.e., the world's last line of defense against resistant pathogens, making these of extreme importance from the environmental point of view [7]. Vancomycin was detected in French rivers in concentrations reaching up to 90 ng L^{-1} [8], and in the effluents of the wastewater treatment plants (WWTPs) of Milan and Varese, Italy, as high as 17.4 ± 1.7 ng L^{-1} and 24.4 ± 31 ng L^{-1}, respectively [9].

Incomplete removal of antibiotics and other drugs from wastewaters at WWTPs requires alternative or supplementary approaches, such as, e.g., advanced oxidation processes (AOPs) using reactive oxygen species (ROS), including atomic oxygen, hydroxyl, and other radicals, able to degrade organic contaminants in water [3,10]. For example, the application of UV/TiO$_2$ combination showed 89.5% degradation of VMN in 36 min at the initial concentration of 58 mg L^{-1}, TiO$_2$ dosage of 55 mg L^{-1}, and temperature 40 °C [11].

Advanced oxidation methods include, among others, UV-induced oxidation and non-thermal electric discharge plasma. Photolysis is used for the activation of extrinsic oxidants such as hydrogen peroxide (HP), peroxydisulfate (PDS), and peroxymonosulfate (PMS) to produce hydroxyl (HO$^{\bullet}$) or sulfate radicals (SO$_4^{\bullet-}$) [12]. Compared with HO$^{\bullet}$, SO$_4^{\bullet-}$ possess equal or even higher redox potential of 2.5–3.1 V and exhibits higher selectivity at longer

half-life [13]. Numerous studies showed high efficacy in degradation and mineralization of contaminants of emerging concern by UV/HP, UV/PDS, and UV/PMS processes [3,13–15].

Non-thermal plasma generates hydroxyl radicals in a variety of electric discharge types [16]. The gas-phase pulsed corona discharge (PCD) is applied to the water dispersed in the form of droplets, jets, and films in the discharge zone. This discharge surpasses other plasma types in energy efficiency due to the formation of hydroxyl radicals at the surface of the treated aqueous solution, i.e., in close vicinity of the target pollutants experiencing negligible resistance in diffusion into the aqueous phase [17]. Except for hydroxyl radicals, atomic oxygen, ozone, hydrogen peroxide, and other reactive species participate in PCD oxidation. Previously, it showed high removal efficiency for pharmaceuticals such as metformin, tramadol, and dexamethasone [18,19], as well as improved oxidation rates with persulfate addition [20]. The use of persulfate additives is actively studied for other plasma types, for example, double barrier discharge, achieving increased degradation rates for different organic pollutants [21–23].

The current study aimed to evaluate the effect of extrinsic oxidants on the degradation and mineralization of VMN in combination with UV photolysis and PCD. To the best of the authors' knowledge, no similar research has been performed, both in terms of the target compound and the use of combinations. Operation parameters, pH, and extrinsic oxidant dose were evaluated for cost efficiency according to the delivered energy and the cost of extrinsic oxidants.

2. Results and Discussion

2.1. Effect of pH on VMN Oxidation in UV Photolysis and PCD Treatment

In blank VMN hydrolysis experiments at unadjusted pH without applying UV or PCD, no significant changes ($\leq 5\%$) in concentration of VMN were observed in 2 h. In turn, the application of direct UV photolysis and PCD treatment resulted in 90% removal at about 0.53 kWh m^{-3} and 0.09 kWh m^{-3} of delivered energy (Figure 1). Thus, the PCD oxidation of VMN was a few times more energy efficient than in UV photolysis.
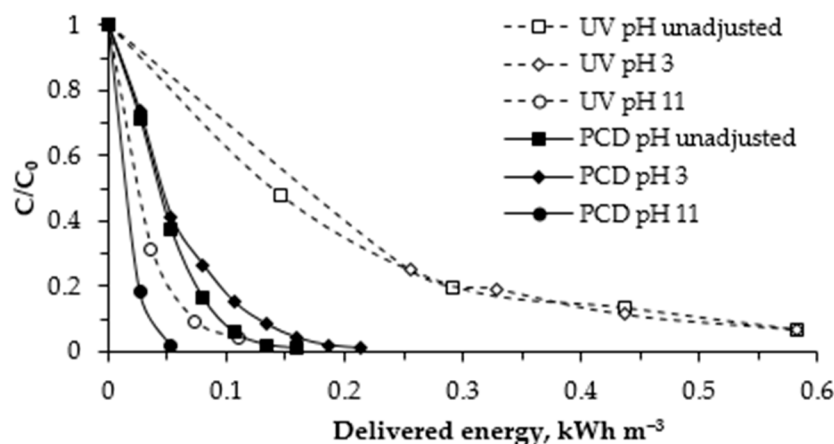

Figure 1. Degradation of VMN at different pH values in UV photolysis and PCD treatment ([VMN]$_0$ = 13.5 µM).

The effect of pH on the oxidation of organic molecules is often associated with their dissociation or protonation. Due to its molecular structure containing numerous deprotonated moieties available for the electrophilic attack [24], the VMN molecule has several dissociation constants making the increase in pH from 2.9 to 11.7, greatly improving its oxidation rate. As shown in Figure 1, the effect of pH on VMN oxidation within acidic to circum-neutral, i.e., the unadjusted conditions interval was negligible for both PCD and UV photolysis processes. However, in alkaline solutions, both processes showed increased oxidation efficacy providing >90% VMN degradation at energy doses lower than in acidic media for 2.5 and 6.0 times in PCD and UV photolysis, respectively. The results of PCD

oxidation are consistent with the study by Dodd et al. [24] where VMN degradation rates in ozonation increased at alkaline pH. This may be also explained with decomposition of ozone-forming hydroxyl radicals at faster rates. The change in pH may also affect the light absorbance properties of the compound, improving it with increasing pH and thus explaining the increased efficiency of UV photolysis at pH 11 [25].

　　　Due to the negligible difference in oxidation rates between acidic and circum-neutral pH, UV/oxidant and PCD/oxidant combinations were studied only in alkaline and neutral solutions. In addition, unadjusted circum-neutral pH decreases during the treatment of VMN solutions due to acidic by-products formation. In PCD treatment, nitrates are formed with nitrogen oxidation [26].

2.2. VMN Oxidation in UV/Oxidant and PCD/Oxidant Combinations

　　　Experiments with oxidants without application of UV irradiation and PCD showed no effect on VMN. Figure 2, Figures S1 and S2 from Supplementary Materials demonstrate the kinetics of VMN degradation in the pseudo-first-order reaction for UV and PCD treatment with and without extrinsic oxidants ($R^2 > 0.98$).
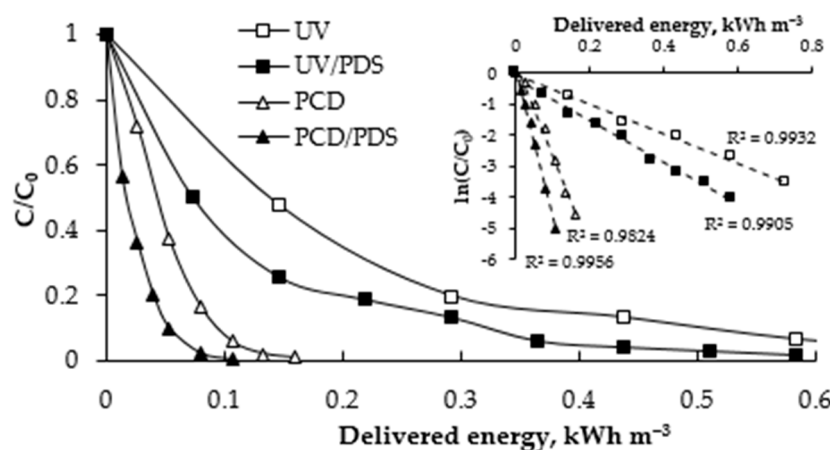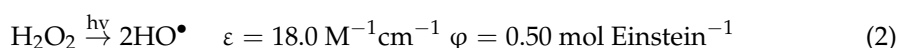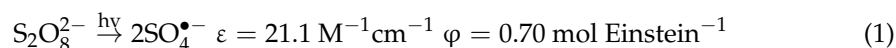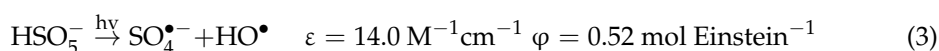

Figure 2. Degradation of VMN in UV photolysis, PCD treatment, UV/PDS, and PCD/PDS combinations ([VMN]$_0$ = 13.5 μM, [PDS]$_0$ = 67.5 μM, unadjusted pH).

　　　For example, the addition of PDS in the amount of 67.5 μM, i.e., in the VMN/PDS molar ratio of 1/5 to UV-irradiated VMN solution, showed synergetic growth of k_1 value 1.43 times from 4.7 to 6.7 m^3 kW^{-1} h^{-1}. For the PCD treatment, the addition of PDS in the same amount improved the reaction rate constant 1.57 times from 30.3 to 47.7 m^3 kW^{-1} h^{-1}. The enhanced VMN degradation may be attributed to the activation of PDS to strong reactive species, $HO^\bullet$ and $SO_4^{\bullet-}$.

　　　Similar VMN degradation enhancement was observed with extrinsic HP and PMS in combinations with UV and PCD (Figures S1 and S2 from Supplementary Materials), showing, however, certain quantitative difference: in the UV photolysis, the addition of 67.5 μM of hydrogen peroxide resulted in $k_1 = 8.8$ m^3 kW^{-1} h^{-1} surpassing the combination with PDS (6.7 m^3 kW^{-1} h^{-1}) and PMS (5.3 m^3 kW^{-1} h^{-1}). The effect of PMS additions on the UV photolysis was of minor importance (Figure S2 from Supplementary Materials), although both oxidants, HP and PMS, exhibited a noticeable yet moderate synergy effect on PCD oxidation (Figure S1 from Supplementary Materials). The reason for this difference is most likely related to the different extrinsic oxidants' activation mechanisms: UV photolysis activates the oxidants by the fission of the O-O bond providing a mixture of sulfate and hydroxyl radicals (Equations (1)–(3)) [13,27]:

$$S_2O_8^{2-} \xrightarrow{h\nu} 2SO_4^{\bullet-} \quad \varepsilon = 21.1 \text{ M}^{-1}\text{cm}^{-1} \quad \varphi = 0.70 \text{ mol Einstein}^{-1} \tag{1}$$

$$H_2O_2 \xrightarrow{h\nu} 2HO^\bullet \quad \varepsilon = 18.0 \text{ M}^{-1}\text{cm}^{-1} \quad \varphi = 0.50 \text{ mol Einstein}^{-1} \tag{2}$$

$$\text{HSO}_5^- \xrightarrow{h\nu} \text{SO}_4^{\bullet-} + \text{HO}^\bullet \quad \varepsilon = 14.0\ \text{M}^{-1}\text{cm}^{-1}\ \varphi = 0.52\ \text{mol Einstein}^{-1} \tag{3}$$
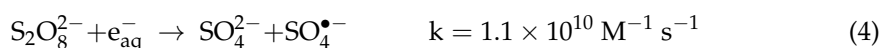
where ε is the molar extinction coefficient at a wavelength of 254 nm, and φ is the quantum yield for UV photolysis.
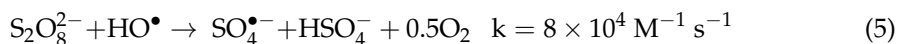
Activation of extrinsic oxidants in PCD proceeds via a complex action of electromagnetic field, UV radiation, and formation of hydroxyl radicals and other reactive species acting as activators. Contrary to UV photolysis, the activation in PCD occurs at the plasma–liquid interface with a minor contribution of reactions in the bulk solution [28].

In PCD, UV light is emitted by the $\text{C}^3\Pi_\text{u} \to \text{B}^3\Pi_\text{g}$ electronic transition in the N_2 molecule and the reported wavelengths for pulsed corona discharge of point-to-plane configuration are above 300 nm [29]. Considering the effective wavelengths activating extrinsic oxidants from 200 to 310 nm, the radiation emitted by PCD most probably plays a negligible role in their activation [13,30].
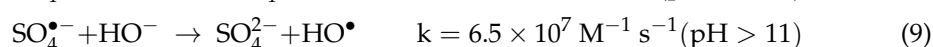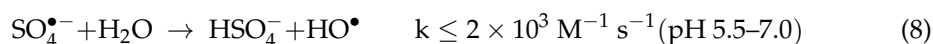
In water radiolysis experiments, a solvated electron (e_aq^-) rapidly activates peroxydisulfate anion (Equation (4)) [31]:

$$\text{S}_2\text{O}_8^{2-} + \text{e}_\text{aq}^- \to \text{SO}_4^{2-} + \text{SO}_4^{\bullet-} \qquad k = 1.1 \times 10^{10}\ \text{M}^{-1}\ \text{s}^{-1} \tag{4}$$
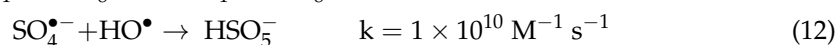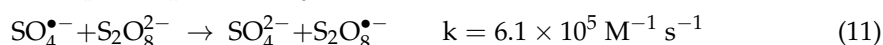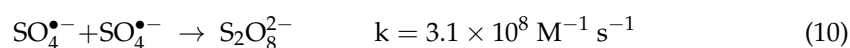
The presence of solvated electrons in atmospheric-pressure plasmas was confirmed by Rumbach et al. [32]. They found an average penetration depth of electrons to water of 2.5 ± 1.0 nm and noted that the kinetics of electron scavenging is similar, although not identical, to the solvated electrons formed in water radiolysis. The extrinsic oxidants' activation mechanism with solvated electrons is presumably the most important one since the rate of PDS activation by ROS (Equations (5)–(7)) is several orders of magnitude lower [22]:
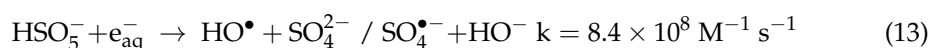
$$\text{S}_2\text{O}_8^{2-} + \text{HO}^\bullet \to \text{SO}_4^{\bullet-} + \text{HSO}_4^- + 0.5\text{O}_2 \quad k = 8 \times 10^4\ \text{M}^{-1}\ \text{s}^{-1} \tag{5}$$

$$\text{S}_2\text{O}_8^{2-} + \text{H}^\bullet \to \text{SO}_4^{\bullet-} + \text{SO}_4^{2-} + \text{H}^+ \qquad k = 2.5 \times 10^7\ \text{M}^{-1}\ \text{s}^{-1} \tag{6}$$

$$\text{S}_2\text{O}_8^{2-} + \text{O}_2^{\bullet-} \to \text{SO}_4^{\bullet-} + \text{SO}_4^{2-} + \text{H}^+ \qquad k = 2.4 \times 10^3\ \text{M}^{-1}\ \text{s}^{-1} \tag{7}$$

The reaction described in Equation (6) is less probable for hydrogen radicals being scavenged at the gas–liquid interface by abundant oxygen. Sulfate radicals formed this or that way, however, are more selective than hydroxyl radicals and may not be utilized in reactions with organic compounds. Instead, sulfate radicals react with water molecules forming hydroxyl radicals in reactions strongly dependent on pH (Equations (8)–(9)) [33,34]:

$$\text{SO}_4^{\bullet-} + \text{H}_2\text{O} \to \text{HSO}_4^- + \text{HO}^\bullet \qquad k \leq 2 \times 10^3\ \text{M}^{-1}\ \text{s}^{-1}(\text{pH } 5.5\text{–}7.0) \tag{8}$$

$$\text{SO}_4^{\bullet-} + \text{HO}^- \to \text{SO}_4^{2-} + \text{HO}^\bullet \qquad k = 6.5 \times 10^7\ \text{M}^{-1}\ \text{s}^{-1}(\text{pH} > 11) \tag{9}$$
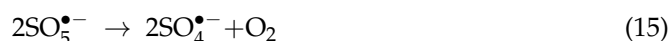
The recombination of sulfate radicals and their reactions with other radicals are faster (Equations (10)–(12)) making these more probable [35,36], hindering the actions of sulfate and hydroxyl radicals:

$$\text{SO}_4^{\bullet-} + \text{SO}_4^{\bullet-} \to \text{S}_2\text{O}_8^{2-} \qquad k = 3.1 \times 10^8\ \text{M}^{-1}\ \text{s}^{-1} \tag{10}$$

$$\text{SO}_4^{\bullet-} + \text{S}_2\text{O}_8^{2-} \to \text{SO}_4^{2-} + \text{S}_2\text{O}_8^{\bullet-} \qquad k = 6.1 \times 10^5\ \text{M}^{-1}\ \text{s}^{-1} \tag{11}$$

$$\text{SO}_4^{\bullet-} + \text{HO}^\bullet \to \text{HSO}_5^- \qquad k = 1 \times 10^{10}\ \text{M}^{-1}\ \text{s}^{-1} \tag{12}$$

The activation of peroxymonosulfate anions introduced with PMS or formed from PDS in PCD presents another concern. The anion HSO_5^- has an asymmetrical structure with the O-O bond having the dissociation energy of 377 kJ mol^{-1} vs. 92 kJ mol^{-1} of peroxydisulfate anion [37], making the HSO_5^- activation via direct cleavage of O-O less probable than that of $\text{S}_2\text{O}_8^{2-}$ (Equation (13)):

$$\text{HSO}_5^- + \text{e}_\text{aq}^- \to \text{HO}^\bullet + \text{SO}_4^{2-}\ /\ \text{SO}_4^{\bullet-} + \text{HO}^-\ k = 8.4 \times 10^8\ \text{M}^{-1}\ \text{s}^{-1} \tag{13}$$
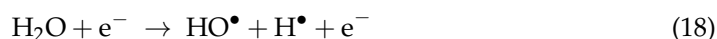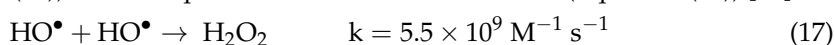
Nevertheless, Shang et al. [37] showed performance of PMS surpassing that of PDS in accelerating oxidation of sulfamethoxazole by dielectric barrier discharge (DBD). They supposed faster oxidation was contributed by the activation of PMS with dissolved ozone (Equations (14)–(16)) [38]:

$$-O_3SOO^- + O_3(aq) \rightarrow -O_3SO_5^- \rightarrow SO_5^{\bullet-} + O_3^{\bullet-} \quad k = 2.2 \times 10^4 \text{ M}^{-1}\text{ s}^{-1} \tag{14}$$

$$2SO_5^{\bullet-} \rightarrow 2SO_4^{\bullet-} + O_2 \tag{15}$$

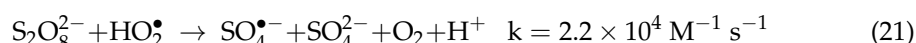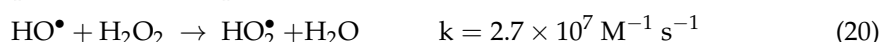$$SO_5^{\bullet-} + O_3 \rightarrow SO_4^{\bullet-} + 2O_2 \tag{16}$$

Due to a relatively slow rate (Equation (14)), the reaction with dissolved ozone formed in PCD [28] likely takes place in the bulk solution.

Concerning hydrogen peroxide, Tikker et al. [20] showed that PCD results in H_2O_2 formation in concentrations of up to 0.11 mM in acidic solutions in 1 h of treatment at the pulsed power of 32 W. The H_2O_2 formation is associated with the hydroxyl radicals' recombination (Equation (17)), which is produced from water molecules (Equation (18)) [37]:
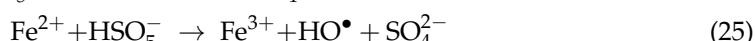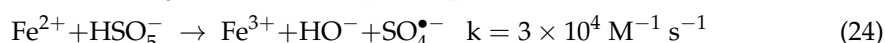
$$HO^\bullet + HO^\bullet \rightarrow H_2O_2 \quad k = 5.5 \times 10^9 \text{ M}^{-1}\text{ s}^{-1} \tag{17}$$

$$H_2O + e^- \rightarrow HO^\bullet + H^\bullet + e^- \tag{18}$$

Sulfate and hydroxyl radicals may also react with HP producing hydroperoxyl radicals ($HO_2^\bullet$) able to activate persulfate anion (Equations (19)–(21)) [33]:

$$SO_4^{\bullet-} + H_2O_2 \rightarrow SO_4^{2-} + HO_2^\bullet + H^+ \quad k = 1.2 \times 10^7 \text{ M}^{-1}\text{ s}^{-1} \tag{19}$$

$$HO^\bullet + H_2O_2 \rightarrow HO_2^\bullet + H_2O \quad k = 2.7 \times 10^7 \text{ M}^{-1}\text{ s}^{-1} \tag{20}$$

$$S_2O_8^{2-} + HO_2^\bullet \rightarrow SO_4^{\bullet-} + SO_4^{2-} + O_2 + H^+ \quad k = 2.2 \times 10^4 \text{ M}^{-1}\text{ s}^{-1} \tag{21}$$

Notably, moderate amounts of ferrous cations form in the stainless steel PCD reactor reaching Fe^{2+} concentrations of up to 0.2 mg L^{-1} within 2 h of treatment. It makes the Fenton reaction (Equation (22)) play a part, presumably minor, in the oxidation mechanism of the target compound in the PCD process.
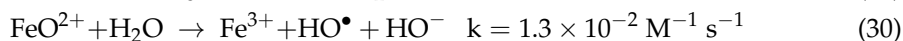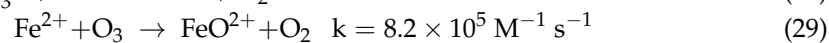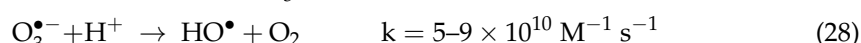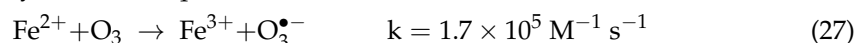
$$Fe^{2+} + H_2O_2 \rightarrow Fe^{3+} + HO^- + HO^\bullet \quad k = 53 \text{ M}^{-1}\text{ s}^{-1} \tag{22}$$
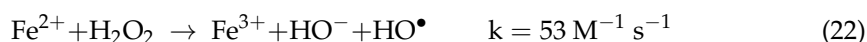
Activation of PDS and PMS with ferrous ions is actively studied (Equations (23)–(25)) [39]:

$$Fe^{2+} + S_2O_8^{2-} \rightarrow Fe^{3+} + SO_4^{2-} + SO_4^{\bullet-} \quad k = 30 \text{ M}^{-1}\text{ s}^{-1} \tag{23}$$

$$Fe^{2+} + HSO_5^- \rightarrow Fe^{3+} + HO^- + SO_4^{\bullet-} \quad k = 3 \times 10^4 \text{ M}^{-1}\text{ s}^{-1} \tag{24}$$

$$Fe^{2+} + HSO_5^- \rightarrow Fe^{3+} + HO^\bullet + SO_4^{2-} \tag{25}$$

Shang et al. [22] reported somewhat accelerated *p*-nitrophenol (2.5 mM) oxidation in the combination of DBD/PDS with the addition of 3.6 μM of Fe^{2+}. A tenfold increase in Fe^{2+} dose modestly accelerated oxidation rate, which may be explained by rapid scavenging of sulfate radicals with excessive ferrous ions (Equations (26)) [22]:

$$SO_4^{\bullet-} + Fe^{2+} \rightarrow Fe^{3+} + SO_4^{2-} \quad k = 4.6 \times 10^9 \text{ M}^{-1}\text{ s}^{-1} \tag{26}$$
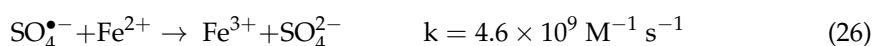
Besides Fenton-like reactions, leaching iron may also catalyze ozone decomposition, producing hydroxyl radicals (Equations (27)–(30)) [40]:

$$Fe^{2+} + O_3 \rightarrow Fe^{3+} + O_3^{\bullet-} \quad k = 1.7 \times 10^5 \text{ M}^{-1}\text{ s}^{-1} \tag{27}$$

$$O_3^{\bullet-} + H^+ \rightarrow HO^\bullet + O_2 \quad k = 5\text{–}9 \times 10^{10} \text{ M}^{-1}\text{ s}^{-1} \tag{28}$$

$$Fe^{2+} + O_3 \rightarrow FeO^{2+} + O_2 \quad k = 8.2 \times 10^5 \text{ M}^{-1}\text{ s}^{-1} \tag{29}$$

$$FeO^{2+} + H_2O \rightarrow Fe^{3+} + HO^\bullet + HO^- \quad k = 1.3 \times 10^{-2} \text{ M}^{-1}\text{ s}^{-1} \tag{30}$$

2.2.1. Effect of Extrinsic Oxidant Dose on VMN Oxidation in UV/Oxidant Combinations

Figure 3 presents the effect of extrinsic oxidant dose, expressed as VMN/oxidant molar ratio, and pH on the reaction rate constant k_1 and TOC removal in VMN oxidation

by unassisted UV photolysis and the UV/oxidant combinations. In the UV photolysis, the k_1 values in circum-neutral and acidic solutions were similarly low, while having TOC elimination slightly increased with decreasing pH. At alkaline pH, the k_1 and TOC degradation achieved the highest values of 29.8 m^3 kW^{-1} h^{-1} and 24.1%, respectively.
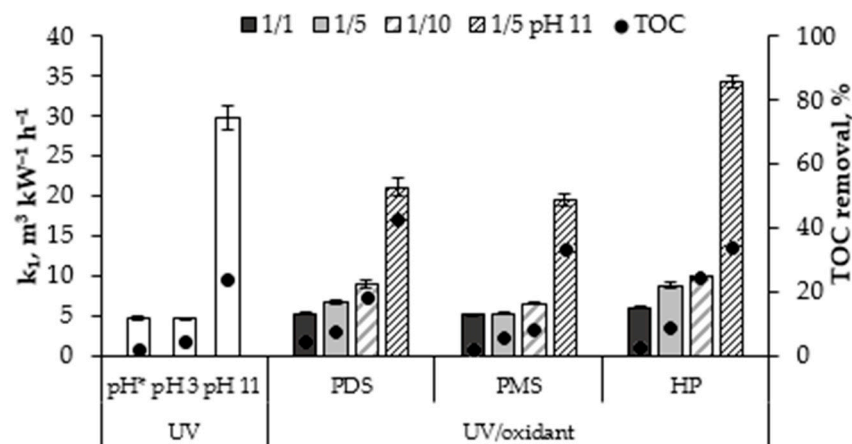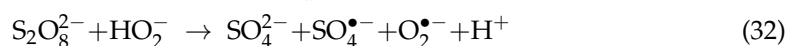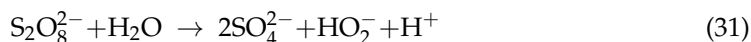

Figure 3. Effects of pH and VMN/oxidant molar ratio on the target compound UV photolytic oxidation rate constant k_1 and TOC removal ([VMN]$_0$ = 13.5 µM, unadjusted pH*, treatment time for TOC removal 2 h).

The performance of the combined treatment in unadjusted pH conditions was moderately enhanced with the increasing extrinsic oxidant concentrations. For instance, the PDS addition in the molar VMN/oxidant ratios of 1/1 (13.5 µM), 1/5 (67.5 µM), and 1/10 (135.0 µM) resulted in the k_1 value increased by 12.2%, 41.3%, and 89.2%, respectively, compared with the unassisted UV photolysis. A similar trend was observed with the UV/HP combination, while the addition of PMS showed low performance achieving only 37.8% in the best k_1 improvement at the 1/10 VMN/PMS molar ratio. These results are consistent with the different molar extinction coefficients presumably resulting in different amounts of produced radicals (Equations (1)–(3)): slower activation of PMS at the fast degradation of VMN by unassisted UV photolysis resulted in a smaller effect of PMS addition.
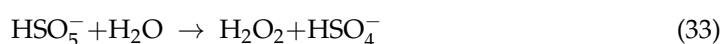
The VMN mineralization was also improved with extrinsic oxidants (Figure 3). The UV/oxidant combinations showed an increase in TOC removal from 1.7% in unassisted UV photolysis in circum-neutral solutions to 18.1%, 24.2%, and 7.9%, respectively, in UV/PDS, UV/HP, and UV/PMS combinations at the oxidant concentrations of 135.0 µM. These observations suggest hydroxyl radicals produced from H_2O_2 are utilized in the oxidation of degradation by-products more effectively for their unselective reactions.

At pH 11, the VMN degradation rate constant k_1 in the unassisted UV photolysis, and UV/PDS and UV/PMS combinations at the VMN/oxidant molar ratio of 1/5 comprised 29.8 m^3 kW^{-1} h^{-1}, 21.1 m^3 kW^{-1} h^{-1}, and 19.5 m^3 kW^{-1} h^{-1}, respectively (Figure 3). The reason for lower oxidation rates in UV/PDS and UV/PMS combinations may be the absorption of the photons by persulfate or peroxymonosulfate anions preventing deprotonated VMN direct photolytic degradation, which is faster than that proceeding via formation of sulfate radicals. The use of the UV/HP combination resulted in k_1 being increased to 34.3 m^3 kW^{-1} h^{-1}, which was probably due to the faster degradation of hydrogen peroxide and production of hydroxyl radicals, thus overpowering their lower oxidation potential in alkaline media [41]. The TOC removal also rose from 24.1% to 33.9% in UV-irradiated alkaline VMN solution with HP addition, which is similar to the improvement at unadjusted circum-neutral pH. The UV/PDS combination showed better performance in TOC removal than UV/PMS, 42.6% vs. 33.0%, due to faster synergism of both VMN photolysis (Figure 1) and PDS decomposition (Equation (5)) in alkaline conditions. The synergy is supported by the persulfate anion activation with hydroperoxide anion-producing sulfate radicals

contributing to the mineralization of VMN oxidation products (Equations (31) and (32)) [13]. Further transformation of sulfate radicals to hydroxyl radicals through Equation (9) may also somewhat change the balance between ionic and molecular forms of VMN and its oxidation by-products affecting further oxidation.

$$S_2O_8^{2-} + H_2O \rightarrow 2SO_4^{2-} + HO_2^- + H^+ \tag{31}$$

$$S_2O_8^{2-} + HO_2^- \rightarrow SO_4^{2-} + SO_4^{\bullet-} + O_2^{\bullet-} + H^+ \tag{32}$$

The activation of PMS in alkaline solutions can also take place, producing hydroxyl radicals, singlet ozone, and superoxide radicals. For example, the degradation of Acid Orange 7 was observed for the alkali/PMS combination but not for the alkali/PDS [42]. One of the important steps of PMS activation at alkaline pH is the formation of hydrogen peroxide and its hydrolysis to hydroperoxide anion, which further produces other ROS (Equations (33)–(35)) [42]:

$$HSO_5^- + H_2O \rightarrow H_2O_2 + HSO_4^- \tag{33}$$

$$H_2O_2 \rightarrow HO_2^- + H^+ \tag{34}$$

$$H_2O_2 + HO^- \rightarrow HO_2^- + H_2O \tag{35}$$

For example, hydrogen peroxide formed in the reaction described by Equation (33) may also be degraded by UV radiation forming hydroxyl radicals (Equation (2)), thus oxidizing VMN and its degradation products. This hypothesis may be evidenced by mineralization with UV/HP proceeding with efficiency similar to the one of PMS in alkaline solutions (Figure 3).

2.2.2. Effect of Extrinsic Oxidant Dose on VMN Oxidation in PCD/Oxidant Combinations

In acidic media, the unassisted PCD treatment showed a somewhat decreased VMN degradation reaction rate constant compared with the unadjusted circum-neutral pH, although the TOC removal increased from 76.9% to 85.7% with decreasing pH (Figure 4). The higher oxidational potential of hydroxyl radicals in acidic media [41] most probably contributed to more effective oxidation, whereas selective reactions of more stable molecular ozone may be attributed to the lower oxidation rate of VMN in acidic solutions. These contrary phenomena resulted in a decreased VMN oxidation rate, although the reaction products, such as oxalate, are easier oxidized in acidic medium providing deeper mineralization [20]. At alkaline pH, similarly to unassisted UV photolysis, the value of k_1 increased to 75.8 m^3 kW^{-1} h^{-1}, while TOC removal decreased by almost half to 48.8%. Similar results were obtained by Tikker et al. [20] for oxalate mineralization in unassisted PCD treatment, and the decreased TOC removal was explained by (i) the decreased hydroxyl radical oxidation potential [41], (ii) scavenging of hydroxyl radicals by carbonates and/or bicarbonates, and (iii) possible scavenging of hydroxyl radicals by ozone. Carbonates/bicarbonates are accumulated in alkaline solutions due to absorption from the air (Equations (36) and (37)) and mineralization of by-products.
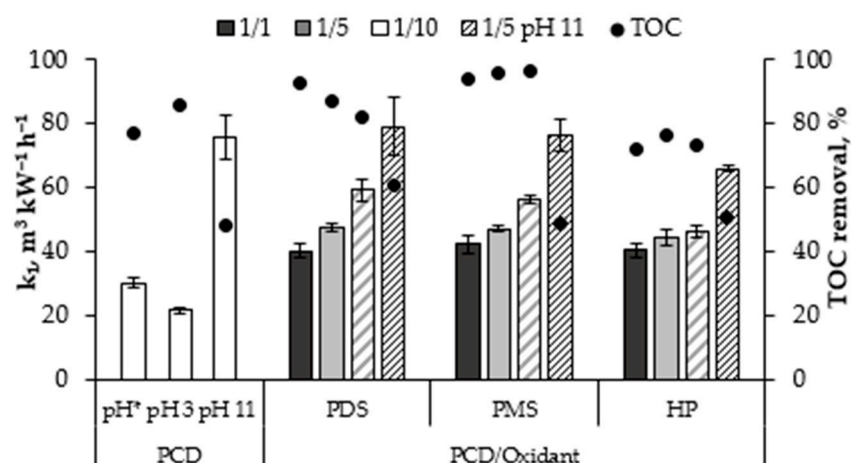
$$CO_2 + HO^- \rightarrow HCO_3^- \tag{36}$$

$$HCO_3^- + HO^- \rightarrow CO_3^{2-} + H_2O \tag{37}$$
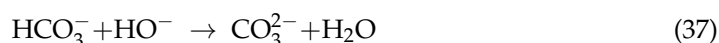
Figure 4. Effect of pH and VMN/oxidant molar ratio on the target compound PCD oxidation rate constant k_1 and TOC removal ($[VMN]_0$ = 13.5 μM, unadjusted pH*, treatment time for TOC removal 2 h).

Table 1 shows the TIC concentration after 2 h of treatment in acidic/circum-neutral and alkaline conditions. In alkaline media, the total inorganic carbon changed during the treatment from around $TIC_0 = 7 \pm 1.4$ to 14 ± 0.7 mg C L^{-1} corresponding to 35 ± 7.0 and 70 ± 3.5 mg L^{-1} of bicarbonate/carbonate, while at the starting circum-neutral pH, the final concentration of bicarbonates did not exceed 4 mg L^{-1} since the pH was reduced during the treatment. The second-order reaction rate constants of radical scavenging reactions with bicarbonates/carbonates are high enough to reduce the number of available hydroxyl radicals and, also, interrupt the formation of ozonide ion radicals from superoxide radicals responsible for the generation of hydroxyl radicals (Equations (38)–(41)) [34]:
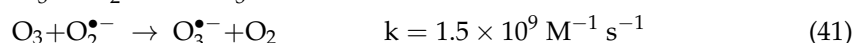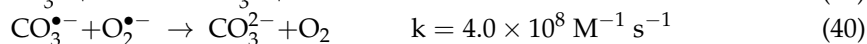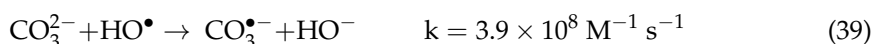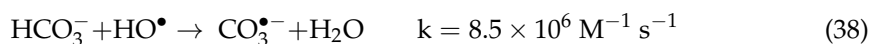
$$HCO_3^- + HO^\bullet \rightarrow CO_3^{\bullet-} + H_2O \qquad k = 8.5 \times 10^6 \text{ M}^{-1} \text{ s}^{-1} \tag{38}$$

$$CO_3^{2-} + HO^\bullet \rightarrow CO_3^{\bullet-} + HO^- \qquad k = 3.9 \times 10^8 \text{ M}^{-1} \text{ s}^{-1} \tag{39}$$

$$CO_3^{\bullet-} + O_2^{\bullet-} \rightarrow CO_3^{2-} + O_2 \qquad k = 4.0 \times 10^8 \text{ M}^{-1} \text{ s}^{-1} \tag{40}$$

$$O_3 + O_2^{\bullet-} \rightarrow O_3^{\bullet-} + O_2 \qquad k = 1.5 \times 10^9 \text{ M}^{-1} \text{ s}^{-1} \tag{41}$$

Table 1. Concentration of TIC in VMN solutions in 2 h of treatment dependent on pH values ($[VMN]_0$ = 13.5 μM, $[oxidant]_0$ = 67.5 μM).

Combination	TIC, mg C L^{-1}	
	pH 3/Unadjusted pH	pH 11
UV	0.5	3.6
UV/PDS	0.8	5.8
UV/HP	1.3	4.3
UV/PMS	0.7	4.7
PCD	0.6	14.3
PCD/PDS	0.6	12.9
PCD/HP	0.6	14.6
PCD/PMS	0.5	13.5

At alkaline pH, ozone may react with hydroxyl radicals forming less reactive hydroperoxyl radicals (Equation (42)) [34]:

$$O_3 + HO^\bullet \rightarrow HO_2^\bullet + O_2 \qquad k = 1.0 \times 10^8 \text{ M}^{-1} \text{ s}^{-1} \tag{42}$$
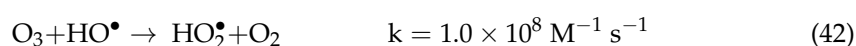
The dose of added oxidants directly affects the oxidation performance in tested combinations, with excessive concentrations exhibiting a self-scavenging effect, whereas a lack of oxidant shows a negligible effect. Previously, the optimum target compound-to-oxidant molar ratio in DBD treatment of benzotriazole and sulfamethoxazole solutions was found to fit into a 1/30–1/40 interval [23,43]. For oxalate, however, oxidation in PCD showed the optimal molar ratio with PDS of 1/0.5, improving the energy efficiency of mineralization for 1.7 times.

In this study, the performance of PCD/oxidant combinations in circum-neutral solutions moderately improved with increased concentrations of extrinsic oxidants following the descending order PCD/PDS > PCD/PMS > PCD/HP (Figure 4), suggesting more effective production of radicals in the PCD/PDS combination. The moderate character of oxidation enhancement is seen from, for example, a less than twofold increase in VMN degradation rate when PDS was added in the amount of tenfold the VMN content: the k_1 value at its maximum of 59.3 m^3 kW^{-1} h^{-1} was achieved at the PDS dose of 135.0 μM at the VMN/PDS molar ratio of 1/10 compared with 30.3 m^3 kW^{-1} h^{-1} for unassisted PCD treatment. The required time to degrade VMN decreased 2-fold from 4 to 2 min indicating that contact with electrical discharges (Equation (4)) is the main mechanism of PDS activation because long-living oxidants, i.e., ozone, were at low concentrations [26]. The disproportional but direct connection between the extrinsic oxidant dose and the reaction rate indicates that sulfate radicals formed by PCD activation from PDS contribute to VMN oxidation. Further oxidation of the VMN degradation products with sulfate radicals also showed an effect compared with unassisted PCD; thus, TOC removal at the lowest PDS dose of 13.5 μM comprised 92.5%, whereas unassisted PCD removed TOC for 76.9% in circum-neutral solutions (Figure 4). The increased PDS dose showed a negative trend in VMN mineralization with decreasing the TOC removal to 82.1% at the maximum VMN/PDS ratio of 1/10, indicating a scavenging effect of sulfate radicals (Equations (10) and (11)) and/or hydrogen peroxide (Equation (19)).

Contrary to the PCD/PDS process, the PCD/PMS combination demonstrated improvement with growing PMS dose in both the pseudo-first-order VMN degradation reaction constant k_1 and mineralization of VMN oxidation products, reaching 56.4 m^3 kW^{-1} h^{-1} and 96.4%, respectively. The difference in activation pathways of PDS and PMS, as well as in the types of active species, provides better performance of PMS in combination with PCD. Furthermore, the activation of PMS with ozone (Equations (14)–(16)) and ferrous ions (Equations (24) and (25)) may also play an important role in changing the tendency in the oxidation rate and mineralization dependent on the extrinsic oxidant dosing. The activation of PMS with aqueous electrons is two orders of magnitude slower than that of PDS due to the higher O-O bond dissociation energy (Equations (4) and (13)), which makes the number of radical species smaller, thus helping to avoid scavenging associated with sulfate radical recombination seen for PDS (Equations (10) and (11)). Somewhat similar results were reported by Shang et al. [37] for the degradation of sulfamethoxazole in DBD/oxidant combinations: the increase in the reaction rate constant with PMS additions was higher than that with PDS compared with unassisted DBD.

The use of PCD/HP combination resulted in the lowest effect on the k_1 value amongst the studied extrinsic oxidants resulting in 46.1 m^3 kW^{-1} h^{-1} at the highest dose of HP (Figure 4). Since there is an accumulation of HP in PCD, its activation is slow, meaning that PCD is a weak hydrogen peroxide activator. This is consistent with the rather low VMN mineralization degree fluctuating from 71.8% to 76.5%. A large dose of HP did not improve oxidation, which was most likely the consequence of radical self-scavenging reactions.

In alkaline solutions, the PCD/oxidant combinations demonstrated accelerated VMN decomposition and decelerated mineralization compared with circum-neutral and acidic media (Figure 4). The accumulation of TIC (Table 1), supposedly as carbonates at pH 11, and associated oxidant-scavenging reactions were the reason for the lower VMN mineralization. The PMS and HP additions showed neutral effect in mineralization compared with unassisted PCD. In the PCD/PDS combination, however, the TOC removal increased from

47.9% in unassisted PCD to 60.9%, which may be determined by the TIC content decrease from 14.3 to 12.9 mg C L^{-1} in the PCD and PCD/PDS combination, respectively, and the increase in the number of reactive species possibly overpowering the scavenging effect of carbonates.

2.3. Identification of VMN Transformation Products

In addition to the efficiency of degradation and mineralization of the target compound, transformation products (TPs) were identified during the oxidation of VMN by the studied UV- and PCD-based systems using LC-MS analysis.

The results obtained showed that in the case of UV-based systems, the predominant transformation product was TP1 with m/z 716, most likely formed during the dehydroxylation of the VMN molecule (proposed elemental composition $C_{66}H_{73}Cl_2N_9O_{23}$), which was also previously identified by Furia et al. [44] in the oxidation of VMN with a Fenton-based system. In addition, the formation of TP2 with m/z 733 ($C_{66}H_{75}Cl_2N_9O_{25}$) and TP4 with m/z 741 ($C_{66}H_{75}Cl_2N_9O_{26}$) was observed, which suggests the hydroxylation of the VMN molecule. For PCD-based oxidation, traces of TP1, TP2, and TP3 were also found, but TP4 with m/z 758 turned out to be specific and more abundant, which most likely indicates the formation of a polyhydroxylated VMN molecule ($C_{66}H_{77}Cl_2N_9O_{28}$).

2.4. Comparison of Operating Costs

To evaluate energy efficiencies of the treatment systems under the scope, energy yields at 90% conversion of VMN (E_{90}, g kW^{-1} h^{-1}) were calculated as the ratio of the oxidized VMN quantity to the energies consumed by the UV irradiation and PCD treatment together with the cost of extrinsic oxidants [20]. The cost of oxidants was considered as EUR 1.0 kg^{-1}, EUR 1.5 kg^{-1}, and EUR 2.5 kg^{-1} for HP, PDS, and PMS, respectively, including transportation and taxation based on average wholesale prices on the market in 2022. The cost of oxidants was converted to the equivalent energy expense considering the average European non-household electric energy price of EUR 0.125 kW^{-1} h^{-1} [45] dependently on the dose, and added to the total energy expenditure. The calculation results are shown in Table 2.

Table 2. Energy efficiencies of VMN oxidation in UV/oxidant and PCD/oxidant combinations ($[VMN]_0 = 13.5$ μM, unadjusted pH).

	\multicolumn{3}{c}{}	E_{90}, g kW^{-1} h^{-1}			
		UV			PCD	
pH 3		36			146	
Unadjusted pH		36			195	
pH 11		228			540	
Molar ratio	UV/PDS	UV/HP	UV/PMS	PCD/PDS	PCD/HP	PCD/PMS
1/1	37	44	34	250	256	126
1/5	34	52	23	187	196	39
1/10	28	61	18	143	136	21
1/5, pH 11	58	173	40	243	248	40

In the unassisted processes at unadjusted circum-neutral pH, the PCD treatment showed more than five times higher energy efficiency than UV photolysis. At pH 11, PCD and UV processes achieved their highest energy efficiencies of 228 g kW^{-1} h^{-1} and 540 g kW^{-1} h^{-1}, respectively.

The addition of extrinsic oxidants without substantial improvement in the oxidation rate negatively affects the energy efficiency while also making the combined treatment less convenient in terms of chemicals delivery, storing, and handling. However, some combinations with PDS and HP demonstrated considerably increased E_{90} values dependent on the applied oxidant dose; thus, at the lowest PDS and HP doses, combinations with PCD

showed cost efficiencies exceeding the unassisted process for about 1.3 times, decreasing with further extrinsic oxidant additions (Table 2).

The UV/PDS combination at the VMN/PDS molar ratio of 1/1 showed the VMN degradation result similar to the unassisted UV photolysis, although noticeably improving TOC removal (Figure 3). Interestingly, in the UV/HP combination, the trend in the treatment energy efficiency dependent on the HP dose is positive, showing the efficiency increased from 44 g kW^{-1} h^{-1} to 61 g kW^{-1} h^{-1} (Table 2). Showing the k_1 values similar to the ones in the UV/PDS process, the UV/HP combination was more effective due to the hydrogen peroxide cost being 1.5 times smaller than PDS.

Finally, being the most expensive and heaviest extrinsic oxidant (MW = 304 g mol^{-1}), PMS yields to other oxidants in energy efficiency compared with direct photolysis and unassisted PCD (Table 2).

3. Materials and Methods

3.1. Chemicals

Vancomycin hydrochloride (C$_{66}$H$_{75}$Cl$_2$N$_9$O$_{24}$·xHCl, ≥99%), sodium persulfate (Na$_2$S$_2$O$_8$, ≥99%), potassium peroxymonosulfate (Oxone®, KHSO$_5$·0.5KHSO$_4$·0.5K$_2$SO$_4$), hydrogen peroxide (H$_2$O$_2$, PERDROGEN™, ≥30%), potassium iodide (KI, ≥ 99%), sodium bicarbonate (NaHCO$_3$, 99%), and sodium sulfite (Na$_2$SO$_3$, ≥99%) were obtained from Sigma-Aldrich, St. Louis, MO, USA and used without further treatment. Methanol (CH$_3$OH, ≥99%), acetonitrile (CH$_3$CN, LiChrosolv®), and formic acid (CH$_2$O$_2$, 99%) used as eluents were obtained from Merck KGaA, Darmstadt, Germany.

3.2. Pulsed Corona Discharge Equipment

The PCD experiments were conducted in a device made by Flowrox Oy (Finland) with characteristics given in Table 3. The device consists of a PCD stainless steel reactor with the storage tank, pulse generator, and circulation pump with the frequency regulator used to control the pump rotation rate (Figure S3 from Supplementary Materials). The plasma reactor contains an electrode system consisting of high voltage wire electrodes positioned horizontally between two grounded vertical parallel plates. The generator applies high voltage pulses to the electrode system at the pulse repetition frequencies in pulses per second (pps) controlled incrementally as shown in Table 3. The output–input ratio of the pulse generator comprises 65%. Treated solution is dispersed through the perforated plate positioned above the wire electrodes at a certain spray density determined as the flow rate divided by the planar cross-sectional area of the plasma zone, m s^{-1}. After passing the plasma zone, treated solution falls to a storage tank, from where it is circulated back to the top of the reactor.

3.3. Photochemical Equipment

Photochemical experiments were performed in batch mode in a 1 L cylindrical glass reactor. A low-pressure mercury germicidal lamp (11 W, TUV PL-S, Philips, Netherlands) placed in a quartz sleeve inside the reactor was used as a UVC source. The input–output power of the lamp is approximately 32%. The incident photon flux at 254 nm of the lamp used in VMN oxidation comprised 2.55 × 10^{-7} Einstein s^{-1} measured by ferrioxalate actinometry. The lamp was turned on for 10 min before the trial to provide a constant radiation output. A water-cooling jacket was used to maintain constant temperature in the reactor.

3.4. Experimental Procedures

Experiments were carried out at an ambient room temperature of 21 ± 1 °C at the VMN initial concentration of 20 mg L^{-1} or 13.5 μM. The unadjusted water pH values were 5.8 ± 0.2 and 6.8 ± 0.2 for UV and PCD experiments, respectively. For acidic (pH 3) and alkaline (pH 11) conditions, pH was regulated by adding H$_2$SO$_4$ or NaOH in 0.1 to 5.0 M solutions. The effect of PDS, PMS, and HP additions in both photochemical and PCD

experiments were studied at concentrations of 13.5 μM, 67.5 μM, and 135.0 μM, providing the oxidant-to-target compound molar ratio equal to 1, 5, and 10. In experiments with the oxidant additions, the oxidation reaction in samples taken for HPLC-PDA analysis was quenched by adding methanol at the sample-to-CH_3OH volume ratio of 10. For the TOC analysis, sodium sulfite was used at the Na_2SO_3-to-oxidant molar ratio of 10. In the UV/oxidant trials, the VMN solution in the amount of 0.8 L was prepared in bi-distilled water and treated for 2 h with permanent stirring by means of a magnetic stirrer. After the dissolution of the added oxidant, the preheated UVC lamp inserted into the reactor initiated the oxidation.

Table 3. Technical parameters of PCD device.

Parameter	Value
Reactor parameters	
Reactor full volume, L	80
Perforated plate size, mm × mm	565 × 97
Number of perforations	24
Diameter of perforations, mm	3
Water flow rate, L min^{-1}	2–18
Spray density, m s^{-1}	0.002–0.0177
Plasma zone volume, m^3	0.011
Contact surface area at flow rate of 1 m^3 h^{-1}, m^{-1}	130 *
Electrode configuration	
High voltage wire length, m	12
Wire diameter, mm	0.6
Distance between electrodes and grounded plate, mm	17
Distance between high-voltage electrodes, mm	30
Generator characteristics	
Pulse repetition frequency, pps	25, 50, 100, 200, 500, and 800
Output power, W	8–112
Peak voltage, kV	22
Peak current, A	290
Current pulse duration, ns	70
Pulse energy, J	0.14–0.16

* The gas–liquid contact surface was measured using a classical method of sulfite oxidation by air oxygen in the presence of cobalt sulfate catalyst [46].

The stock solutions for PCD experiments were prepared in a 1 L volumetric flask using bi-distilled water, followed by dilution to a total volume of 5 L by distilled water in the reactor tank. Pre-selected amounts of the extrinsic oxidant were dissolved in a 100 mL volumetric flask and mixed with the treated solution in the tank before the start of treatment. All PCD experiments were performed at a circulated water flow rate of 1 m^3 h^{-1} corresponding to the gas–liquid contact surface area of 130 m^{-1} and the pulse repetition frequency of 50 pps with the pulsed power input of 8 W. The plasma treatment time comprised 2 h with a total energy dose of 2.4 kWh m^{-3} delivered to the treated sample. For proper sampling, the treated solutions were circulated in the reactor for four minutes after the pulse generator was turned off for equalizing the concentrations in the reactor's volume.

3.5. Analytical Methods

The concentration of VMN was determined using high-performance liquid chromatography combined with a diode array detector (HPLC-PDA, Shimadzu SPD-M20A, Shimadzu, Kyoto, Japan) equipped with a Phenomenex Gemini (150 × 2.0 mm, 1.7 mm) NX-C18 (110 Å, 5 μm) column. The analysis was performed using an isocratic method with a mobile phase composed of 9% vol. of acetonitrile containing 0.3% of formic acid and

91% vol. of 0.3% formic acid aqueous solution. The flow rate was kept at 0.25 mL min^{-1}. Samples injected in 75 μL volume were analyzed at a wavelength of 220 nm.

Samples from selected experiments were analyzed by high-performance liquid chromatography coupled with a mass spectrometer (HPLC-MS, Shimadzu LC-MS 2020, Shimadzu, Japan). Mass spectra were acquired in the full scan mode (scanning in the range of 100–1500 m/z). The instrument was operated in positive ESI mode and the results obtained with the MS detector were processed using Shimadzu Lab Solutions software.

Total carbon (TC) and total inorganic carbon (TIC) were measured using a TOC analyzer multi N/C® 3100 (Analytik Jena, Jena, Germany) in 20 mL samples with an injection volume of 500 μL for each replicate. Solution pH was measured using a digital pH/Ion meter (Mettler Toledo S220, Mettler Toledo, Greifensee, Switzerland).

Utilization of persulfates was quantified iodometrically measuring residual concentrations in the treated samples by adding an excess KI and using a spectrophotometer (Genesys 10S, Thermo Scientific, Waltham, MA, USA) at $\lambda = 352$ nm [47]. The residual H_2O_2 concentration was measured spectrophotometrically at $\lambda = 410$ nm with titanyl sulfate by a H_2O_2-Ti^{4+} complex formation [48].

Due to different volumes of treated water and power input, photolytic and PCD oxidation processes cannot be compared by observing the decrease in VMN concentration over time, but only by the delivered energy doses calculated for the water volumes and the delivered power in the time of treatment.

To evaluate the effect of extrinsic oxidant addition on the VNM degradation efficiency, a pseudo-first-order reaction rate constant k_1 was calculated (Equation (43)) using slopes of the straight lines by plotting $\ln(C_t/C_0)$ as a function of delivered energy dose D (Equation (44)) through linear regression:

$$\frac{d[C]}{dD} = -k_1 \cdot [C] \tag{43}$$

$$D = \frac{P \cdot t}{V} \tag{44}$$

where k_1—pseudo-first-order reaction rate constant, m^3 kW^{-1} h^{-1}; C—concentration of target compound; D—delivered energy dose, kWh m^{-3}, P—power delivered in PCD or UV treatment, kW; and V—volume of treated solution, m^3.

The energy efficiency E_{90}, g kW^{-1} h^{-1}, was calculated for 90% VMN degradation using Equation (45):

$$E_{90} = \frac{\Delta C \cdot V}{W} \tag{45}$$

where ΔC—a decrease in target compound concentration, g m^{-3}; V—volume of treated solution, m^3; and W—energy consumption derived from the generator power output and the time of treatment, kWh.

4. Conclusions

The UV photolysis, PCD, UV/oxidant, and PCD/oxidant processes were found to be effective in decomposing the aqueous pharmaceutical vancomycin. All studied extrinsic oxidants demonstrated certain synergism with PCD and UV, accelerating oxidation. For all combinations, with a minor exception for UV/PMS showing negligible improvement, an increase in the dose of extrinsic oxidant resulted in a noticeable increase in the pseudo-first-order rate constant. In the UV/oxidant combination, TOC removal increased mostly linearly with the applied oxidant dose, although in the PCD/oxidant combination, the effect of the oxidant dose on TOC removal showed variable deviations, with only the PCD/PMS combination showing a positive trend at the highest removals. The TOC removal in the PCD/oxidant combinations remarkably exceeds the one in the UV/oxidant treatment.

The direct UV photolysis and unassisted PCD demonstrated relatively high energy efficiency of 36 g kW^{-1} h^{-1} and 195 g kW^{-1} h^{-1}, respectively. For all combinations, a positive effect on the energy efficiency was observed only at the lowest oxidants doses,

except for the UV/HP combination which almost doubled the energy efficiency at the VMN/oxidant molar ratio of 1/10 compared with unassisted UV photolysis. In conclusion, the application of UV/HP at higher oxidant doses and PCD/HP and PCD/PDS combinations at moderate oxidant doses provide advantageous VMN degradation and mineralization. On the other hand, the unassisted PCD treatment provides sufficiently high energy efficiency as a chemical-free method.

References

1. Patel, M.; Kumar, R.; Kishor, K.; Mlsna, T.; Pittman, C.U.; Mohan, D. Pharmaceuticals of emerging concern in aquatic systems: Chemistry, occurrence, effects, and removal methods. *Chem. Rev.* **2019**, *119*, 3510–3673. [CrossRef] [PubMed]
2. Larsson, D.G.J. Antibiotics in the environment. *Ups. J. Med. Sci.* **2014**, *119*, 108–112. [CrossRef]
3. Wang, J.; Zhuan, R. Degradation of antibiotics by advanced oxidation processes: An overview. *Sci. Total Environ.* **2020**, *701*, 135023. [CrossRef] [PubMed]
4. Carvalho, I.T.; Santos, L. Antibiotics in the aquatic environments: A review of the European scenario. *Environ. Int.* **2016**, *94*, 736–757. [CrossRef]
5. Cycon, M.; Borymski, S.; Orlewska, K.; Wasik, T.J.; Piotrowska-Seget, Z. An analysis of the effects of vancomycin and/or vancomycin-resistant citrobacter freundii exposure on the microbial community structure in soil. *Front. Microbiol.* **2016**, *7*, 1015. [CrossRef]
6. Gotvajn, A.Ž.; Rozman, U.; Antončič, T.; Urbanc, T.; Vrabel, M.; Derco, J. Fe^{2+} and UV catalytically enhanced ozonation of selected environmentally persistent antibiotics. *Processes* **2021**, *9*, 521. [CrossRef]
7. Okano, A.; Isley, N.A.; Boger, D.L. Peripheral modifications of [Ψ[CH2NH]Tpg4]vancomycin with added synergistic mechanisms of action provide durable and potent antibiotics. *Proc. Natl. Acad. Sci. USA* **2017**, *114*, E5052–E5061. [CrossRef] [PubMed]
8. Tuc Dinh, Q.; Alliot, F.; Moreau-Guigon, E.; Eurin, J.; Chevreuil, M.; Labadie, P. Measurement of trace levels of antibiotics in river water using on-line enrichment and triple-quadrupole LC-MS/MS. *Talanta* **2011**, *85*, 1238–1245. [CrossRef]
9. Zuccato, E.; Castiglioni, S.; Bagnati, R.; Melis, M.; Fanelli, R. Source, occurrence and fate of antibiotics in the Italian aquatic environment. *J. Hazard. Mater.* **2010**, *179*, 1042–1048. [CrossRef] [PubMed]
10. Dulova, N.; Kattel, E.; Trapido, M. Activated Persulfate and Hydrogen Peroxide Treatment of Highly Contaminated Water Matrices: A Comparative Study. *Int. J. Environ. Sci. Develop.* **2020**, *11*, 549–554. [CrossRef]
11. Dehghani, F.; Yousefinejad, S.; Dehghani, M.; Borghei, S.M.; Javid, A.H. Photocatalytic degradation of vancomycin using titanium dioxide and optimization by central composite design. *Int. J. Environ. Sci. Technol.* **2022**, *19*, 8957–8968. [CrossRef]
12. Lee, J.; Von Gunten, U.; Kim, J.H. Persulfate-based advanced oxidation: Critical assessment of opportunities and roadblocks. *Environ. Sci. Technol.* **2020**, *54*, 3064–3081. [CrossRef]
13. Wang, J.; Wang, S. Activation of persulfate (PS) and peroxymonosulfate (PMS) and application for the degradation of emerging contaminants. *Chem. Eng. J.* **2018**, *334*, 1502–1517. [CrossRef]
14. Kaur, B.; Kattel, E.; Dulova, N. Insights into nonylphenol degradation by UV-activated persulfate and persulfate/hydrogen peroxide systems in aqueous matrices: A comparative study. *Environ. Sci. Pollut. Res.* **2020**, *27*, 22499–22510. [CrossRef] [PubMed]
15. Wols, B.A.; Harmsen, D.J.H.; Wanders-Dijk, J.; Beerendonk, E.F.; Hofman-Caris, C.H.M. Degradation of pharmaceuticals in UV (LP)/H_2O_2 reactors simulated by means of kinetic modeling and computational fluid dynamics (CFD). *Water Res.* **2015**, *75*, 11–24. [CrossRef]

16. Malik, M.A. Water purification by plasmas: Which reactors are most energy efficient? *Plasma Chem. Plasma Process.* **2010**, *30*, 21–31. [CrossRef]

17. Ajo, P.; Kornev, I.; Preis, S. Pulsed corona discharge induced hydroxyl radical transfer through the gas-liquid interface. *Sci. Rep.* **2017**, *7*, 16152. [CrossRef] [PubMed]

18. Derevshchikov, V.; Dulova, N.; Preis, S. Oxidation of ubiquitous aqueous pharmaceuticals with pulsed corona discharge. *J. Electrostat.* **2021**, *110*, 103567. [CrossRef]

19. Onga, L.; Kattel-Salusoo, E.; Preis, S.; Dulova, N. Deegradation of anti-inflammatory drug dexamethasone by pulsed corona discharge: The effect of peroxycompounds addition. *J. Environ. Chem. Eng.* **2022**, *10*, 108042. [CrossRef]

20. Tikker, P.; Dulova, N.; Kornev, I.; Preis, S. Effects of persulfate and hydrogen peroxide on oxidation of oxalate by pulsed corona discharge. *Chem. Eng. J.* **2021**, *411*, 128586. [CrossRef]

21. Shang, K.; Wang, X.; Li, J.; Wang, H.; Lu, N.; Jiang, N.; Wu, Y. Synergetic degradation of Acid Orange 7 (AO7) dye by DBD plasma and persulfate. *Chem. Eng. J.* **2017**, *311*, 378–384. [CrossRef]

22. Shang, K.; Li, W.; Wang, X.; Lu, N.; Jiang, N.; Li, J.; Wu, Y. Degradation of p-nitrophenol by DBD plasma/Fe^{2+}/persulfate oxidation process. *Sep. Purif. Technol.* **2019**, *218*, 106–112. [CrossRef]

23. Wu, J.; Xiong, Q.; Liang, J.; He, Q.; Yang, D.; Deng, R.; Chen, Y. Degradation of benzotriazole by DBD plasma and peroxymonosulfate: Mechanism, degradation pathway and potential toxicity. *Chem. Eng. J.* **2020**, *384*, 123300. [CrossRef]

24. Dodd, M.C.; Buffle, M.O.; Von Gunten, U. Oxidation of antibacterial molecules by aqueous ozone: Moiety-specific reaction kinetics and application to ozone-based wastewater treatment. *Environ. Sci. Technol.* **2006**, *40*, 1969–1977. [CrossRef] [PubMed]

25. Shen, Y.-S.; Lin, C.-C. The Effect of pH on the Decomposition of hydrophenols in aqueous solutions by ultraviolet direct photolysis and the ultraviolet-hydrogen peroxide process. *Water Environ. Res.* **2003**, *75*, 54–60. [CrossRef] [PubMed]

26. Kornev, I.; Osokin, G.; Galanov, A.; Yavorovskiy, N.; Preis, S. Formation of nitrite- and nitrate-ions in aqueous solutions treated with pulsed electric discharges. *Ozone Sci. Eng.* **2013**, *35*, 22–30. [CrossRef]

27. Luo, C.; Ma, J.; Jiang, J.; Liu, Y.; Song, Y.; Yang, Y.; Guan, Y.; Wu, D. Simulation and comparative study on the oxidation kinetics of atrazine by UV/H_2O_2, UV/HSO_5^- and $UV/S_2O_8^{2-}$. *Water Res.* **2015**, *80*, 99–108. [CrossRef] [PubMed]

28. Preis, S.; Panorel, I.C.; Kornev, I.; Hatakka, H.; Kallas, J. Pulsed corona discharge: The role of ozone and hydroxyl radical in aqueous pollutants oxidation. *Water Sci. Technol.* **2013**, *68*, 1536–1542. [CrossRef]

29. Mraihi, A.; Merbahi, N.; Yousfi, M.; Abahazem, A.; Eichwald, O. Electrical and spectroscopic analysis of mono- and multi-tip pulsed corona discharges in air at atmospheric pressure. *Plasma Sources Sci. Technol.* **2011**, *20*, 065002. [CrossRef]

30. Sizykh, M.; Batoeva, A.; Tsydenova, O. UV-activated persulfate oxidation of Orange III dye using KrCl excilamp. *Clean Soil Air Water* **2018**, *46*, 1700187. [CrossRef]

31. Neta, P.; Madhavan, V.; Zemel, H.; Fessenden, R.W. Rate constants and mechanism of reaction of SO_4 with aromatic compounds. *J. Am. Chem. Soc.* **1977**, *99*, 163–164. [CrossRef]

32. Rumbach, P.; Bartels, D.M.; Sankaran, R.M.; Go, D.B. The solvation of electrons by an atmospheric-pressure plasma. *Nat. Commun.* **2015**, *6*, 7248. [CrossRef] [PubMed]

33. Chen, N.; Lee, D.; Kang, H.; Cha, D.; Lee, J.; Lee, C. Catalytic persulfate activation for oxidation of organic pollutants: A critical review on mechanisms and controversies. *J. Environ. Chem. Eng.* **2022**, *10*, 107654. [CrossRef]

34. Neta, P.; Huie, R.E.; Ross, A.B. Rate constants for reactions of inorganic radicals in aqueous solution. *J. Phys. Chem. Ref. Data* **1988**, *17*, 1027–1284. [CrossRef]

35. Wang, S.; Zhou, N. Removal of carbamazepine from aqueous solution using sono-activated persulfate process. *Ultrason. Sonochem.* **2016**, *29*, 156–162. [CrossRef] [PubMed]

36. Xie, P.; Ma, J.; Liu, W.; Zou, J.; Yue, S.; Li, X.; Wiesner, M.R.; Fang, J. Removal of 2-MIB and geosmin using UV/persulfate: Contributions of hydroxyl and sulfate radicals. *Water Res.* **2015**, *69*, 223–233. [CrossRef]

37. Shang, K.; Morent, R.; Wang, N.; Wang, Y.; Peng, B.; Jiang, N.; Lu, N.; Li, J. Degradation of sulfamethoxazole (SMX) by water falling film DBD plasma/persulfate: Reactive species identification and their role in SMX degradation. *Chem. Eng. J.* **2022**, *431*, 133916. [CrossRef]

38. Deniere, E.; Van Hulle, S.; Van Langenhove, H.; Demeestere, K. Advanced oxidation of pharmaceuticals by the ozone-activated peroxymonosulfate process: The role of different oxidative species. *J. Hazard. Mater.* **2018**, *360*, 204–213. [CrossRef]

39. Xiao, S.; Cheng, M.; Zhong, H.; Liu, Z.; Liu, Y.; Yang, X.; Liang, Q. Iron-mediated activation of persulfate and peroxymonosulfate in both homogeneous and heterogeneous ways: A review. *Chem. Eng. J.* **2020**, *384*, 123265. [CrossRef]

40. Zeng, Z.; Zou, H.; Li, X.; Arowo, M.; Sun, B.; Chen, J.; Chu, G.; Shao, L. Degradation of phenol by ozone in the presence of Fenton reagent in a rotating packed bed. *Chem. Eng. J.* **2013**, *229*, 404–411. [CrossRef]

41. Wardman, P. Reduction potentials of one electron couples involving free radicals in aqueous solution. *J. Phys. Chem. Ref. Data* **1989**, *18*, 1637–1755. [CrossRef]

42. Qi, C.; Liu, X.; Ma, J.; Lin, C.; Li, X.; Zhang, H. Activation of peroxymonosulfate by base: Implications for the degradation of organic pollutants. *Chemosphere* **2016**, *151*, 280–288. [CrossRef] [PubMed]

43. Wang, Y.; Huang, J.; Guo, H.; Puyang, C.; Han, J.; Li, Y.; Ruan, Y. Mechanism and process of sulfamethoxazole decomposition with persulfate activated by pulse dielectric barrier discharge plasma. *Sep. Purif. Technol.* **2022**, *287*, 120540. [CrossRef]

44. Furia, F.; Minella, M.; Gosetti, M.; Turci, F.; Sabatino, R.; Di Cesare, A.; Corno, G.; Vione, D. Elimination from wastewater of antibiotics reserved for hospital settings, with a Fenton process based on zero-valent iron. *Chemosphere* **2021**, *283*, 131170. [CrossRef] [PubMed]
45. European Commission Eurostat. Electricity Price Statistics-Statistics Explained 2022. Available online: https://ec.europa.eu/eurostat/statistics-explained/index.php/Electricity_price_statistics (accessed on 22 December 2022).
46. Danckwerts, P.V. *Gas-Liquid Reactions*; McGraw-Hill Book Co.: New York, NY, USA, 1970.
47. Liang, C.; Huang, C.F.; Mohanty, N.; Kurakalva, R.M. A rapid spectrophotometric determination of persulfate anion in ISCO. *Chemosphere* **2008**, *73*, 1540–1543. [CrossRef] [PubMed]
48. Eisenberg, G.M. Colorimetric determination of hydrogen peroxide. *Ind. Eng. Chem. Anal. Ed.* **1943**, *15*, 327–328. [CrossRef]